Received: 9 June 2021 | Revised: 6 September 2021 | Accepted: 19 September 2021

DOI: 10.1111/ffe.13588

ORIGINAL ARTICLE

FFEMS Fatigue & Fracture of Engineering Materials & Structures WILEY

Development and validation of a probabilistic model for notch fatigue strength prediction of tool steels based on surface defects

Mattia Zanni | **Alessandro Morri** | **Lorella Ceschini**

Department of Industrial Engineering (DIN), Alma Mater Studiorum – University of Bologna, Bologna, Italy

Correspondence
Mattia Zanni, Department of Industrial Engineering (DIN), Alma Mater Studiorum – University of Bologna, Viale Risorgimento 4, 40136 Bologna, Italy.
Email: mattia.zanni2@unibo.it

Abstract

A new model for the high cycle notch fatigue strength prediction of tool steels subjected to axial loading is proposed, based on previous literatures studies and experimental tests carried out on six different tool steels, including rotating bending fatigue tests on notched specimens, fractographic analyses, hardness, residual stress, and roughness measurements. The novelty is the assumption that surface defects are the main cause of notch fatigue failures of such steels. A probabilistic approach was implemented by modeling size distributions of defects, resulting in the prediction of normal distributions of fatigue strength. Like to other previous models, the effect of steel hardness, surface residual stress, notch severity, and specimen size was also taken into account. Model calibration and validation were performed using the data collected by the experimental activity. Model behavior was investigated by performing a sensitivity analysis, aiming to verify the response to variations of the considered input variables. Prediction errors of only 1.3% (on average) and 3.1% (maximum) resulted from the comparison between model-predicted and experimental notch fatigue strength.

KEYWORDS

fracture mechanics, modeling, notch fatigue strength, surface defects, tool steels

1 | INTRODUCTION

Tool steels are special steels suitable for working or processing of materials. Their in-service performance mainly depends on hardness, toughness, wear, and fatigue resistance.[1–5] Fatigue strength and duration, in particular, are also key factors for their possible application in critical automotive components, such as engine camshafts and crankshafts, typically subjected to cyclic stress conditions.[6] The experimental assessment of fatigue strength requires statistical methods for test planning and analysis of results, such as the *staircase method*,[7] due to the scatter of fatigue data. Due to the great number of required tests, fatigue strength evaluation is a time-consuming as well as costly operation. Consequently, it is desirable to predict the high cycle fatigue strength (or, conversely, the *conventional fatigue limit* for those materials whose S-N curves show a definite knee point in the range at $2{\cdot}10^6$ or 10^7 load cycles, such as steels,[8] if the fatigue behavior at higher number of cycles

is disregarded) from other mechanical properties whose assessment can be simpler and faster. Although empirical relationships between fatigue strength and static properties, such as hardness or ultimate tensile strength, are already available in literature for steels,[9–11] their effectiveness is limited only to relatively low strength steels ($HV \leq 400$[10] or $UTS \leq 1400$ MPa[11]). This lack for high strength steels, such as tool steels, arises from the difference in fatigue crack initiation sites.[9] For low strength steels, if no notable defects are present, fatigue cracks generally nucleate at persistent slip bands on the specimen surface, the formation of which is due to dislocation slip and is closely linked to the strength of the steel.[9] Instead, in high and very high cycle fatigue regimes of high strength steels, crack nucleation occurs at microstructural defects, such as non-metallic inclusions and large carbides, and also occurs at surface defects caused by final machining or surface treatments, such as machining marks, scratches and roughness valleys.[9,10,12–26] Such defects act as stress raisers or pre-existing cracks[10,23,24,27–29] and cause fatigue failures to occur at lower stress levels than those predicted by the currently available empirical relationships reported in literature.[9–11] Furthermore, the statistical distribution of defect size results in an increased scatter of fatigue strength.

It is also worth noting that the above-mentioned equations for fatigue strength prediction do not take into consideration the effect of notches on fatigue strength of tool steels, whereas they are often present in many engineering components, leading to stress intensification and thus reducing fatigue strength.[10,11,26,30] Notch severity is generally quantified through the theoretical stress-concentration factor, K_t, which relates the greatest elastically-calculated stress at the notch-tip to the nominal stress.[31] The effect of surface conditions on the high cycle fatigue strength of tool steels is particularly significant in notched components with high K_t factor, in which the notch leads to high stresses only in a very little surface volume.[9,10,15,17,32] In fact, the outstanding microstructural quality and cleanliness of currently available tool steels result in a negligible effect of microstructural defects on their notch fatigue strength, and thus in a dominant effect of surface defects, such as scratches, machining marks and roughness valleys. This is due to the fact that the production processes of high-performance tool steels, such as electro slag remelting (ESR) and powder metallurgy (PM), result in a very low volume content of microstructural defects of very small size. Hence, the probability that a detrimental microstructural defect exists in the highly stressed, small volume at the notch-tip surface is extremely low. Several criteria for notch fatigue strength assessment are available in the literature, such as methods based on the "theory of critical distance" (TCD),[33–37] stress-field intensity,[38,39] and energy-field[40] approaches, as well as strain-energy density (SED) methods, such as the finite-volume SED.[41–44] However, even if these criteria can consider the detrimental effect of surface defects on the fatigue strength, they do not explicitly assume surface defects as the root cause of high cycle fatigue failures in notched components. Moreover, they often require the knowledge of the whole stress field at the notch-tip, and thus a finite element calculation. Furthermore, the aforementioned criteria do not generally predict distributions of fatigue strength, thus being ineffective in representing the scatter of fatigue strength.

Based on the above and taking into account previous literature studies,[10,12,15,17,25–27,32,45,46] a novel model for the prediction of high cycle notch fatigue strength of tool steels is proposed in the present work, where surface defects (machining marks, scratches and roughness valleys) existing at the notch-tip are explicitly considered as the root cause of high cycle fatigue failures. Size distributions of surface defects were modelled, aiming to compute distributions of fatigue strength and simulate (and possibly predict) the variability of high cycle fatigue strength. As for the already available literature models, the effects of hardness, surface residual stress, notch severity and specimen size were also taken into account. The proposed model was developed and validated on the experimental data collected on six different tool steels, heat treated to a final hardness in the range 640–870 HV. The experimental activity included rotating bending fatigue tests on notched specimens ($K_t = 3$), fractographic analyses, hardness, surface roughness and residual stress measurements. Model effectiveness was assessed by considering the prediction error, defined as the difference between the experimental and the model-predicted notch fatigue strength for the six tool steels. Finally, the behavior of the developed model was characterized by performing a sensitivity analysis.

2 | EXPERIMENTAL ACTIVITY

In the present work, six tool steels (from here indicated as A, B, C, D, E, F) were investigated. All the investigated steels were produced by powder metallurgy (PM) except steel F, manufactured by Electro Slag Remelting (ESR). Table 1 summarizes the average chemical compositions of the steels, evaluated by glow discharge-optical emission spectroscopy (GD-OES, Spectruma GDA 650 HR Analyser) according to ISO14707.[47] As can be noted, steels D and E are characterized by the same chemical composition, but underwent different heat treatments.

TABLE 1 Chemical composition (wt.%) of the investigated tool steels

	Chemical composition (wt.%)									
Steel	**C**	**Cr**	**Mo**	**W**	**V**	**Co**	**Nb**	**Si**	**Mn**	**Fe**
A	1.48	3.94	2.82	2.58	5.62	0.49	0.05	0.65	0.27	bal.
B	0.61	3.70	2.23	2.20	1.69	0.36	0.03	1.26	0.28	bal.
C	0.85	3.78	2.95	3.01	1.31	5.94	1.09	0.66	0.18	bal.
D, E	0.81	4.26	3.03	2.44	2.35	3.98	0.04	0.60	0.36	bal.
F	0.46	4.02	3.09	0.01	0.58	0.24	0.00	0.20	0.24	bal.

TABLE 2 Summary of heat treatment temperatures for each investigated steel

	Temperature (°C)			
Steel	**Austenitizing**	**First and second tempering**	**Sub-zero treatment**	**Third tempering**
A, B, E	1150–1180	510–520	−80	520–530
C, D	1070–1100	540–560	Not performed	540–560
F	1050–1070	540–550	Not performed	540–550

The steels underwent different heat treatment cycles comprising austenitizing (after a double pre-heat at 650°C and 850°C), gas quenching in nitrogen gas (5 bar) and multiple tempering, and an eventual sub-zero treatment at −80°C performed between the second and the last tempering. The performed heat treatment cycles are briefly summarized in Table 2.

Figure 1 reports the microstructures of the investigated steels after heat treatment, obtained using a ZEISS Axio Imager A.1 M optical microscope (OM) on metallographic cross-sections, polished and etched with 2% HNO_3 in ethanol. As can be noted, all the steels exhibited a fine microstructure of tempered martensite, consistent with the chemical compositions and heat treatment cycles reported in Table 1 and Table 2. Moreover, the steels produced by PM (from A to E) also exhibited uniform distributions of fine alloying carbides, resulting from both the manufacturing process and the heat treatment, as described in Roberts et al.[2] Instead, no alloying carbide was observed in steel F, manufactured by ESR. No non-metallic inclusion, large carbide or carbide cluster was observed on the investigated metallographic sections.

Vickers hardness after heat treatment was evaluated according to ISO6507[48] using a 30 kg load and a 10 s duration time. For each steel, Table 3 reports the resulting average value and standard deviation of Vickers hardness HV.

The 10^7 cycles notch fatigue strength at 50% probability of failure was evaluated by performing four point rotating bending tests (nominal stress ratio $R = -1$) according to ISO1143[49] on notched specimens, following the modified staircase method according to ISO12107[7] with a 50 MPa stress step. Figure 2 shows the geometry of fatigue specimens, consistent with ISO1143.[49] Notch geometry was designed to obtain a theoretical stress concentration factor $K_t = 3$ (evaluated using the formulas in Noda and Takase[50]) with an external gage diameter of 5.2 mm, a minimum notch-tip diameter $d_{notch} = 4.02$ mm, a 60° notch angle and a 0.13 mm notch radius. The notch was milling-machined to a target average roughness R_a in the range 0.2–0.3 μm. Roughness profiles were acquired according to DIN4768[51] using a stylus profilometer (tip radius of 5 μm) in order to evaluate the average (R_a) and maximum (R_{max}) roughness. Four roughness profiles were acquired for each specimen. The available equipment did not allow performing roughness measurements on the notch-tip surface along the circumferential direction; hence, roughness profiles were acquired on the notch-flank surface, as shown in Figure 2 (solid red line).

The summary of average (R_a) and maximum (R_{max}) roughness values is reported in Table 4. As can be noted, all the sets of specimens exhibited an average roughness R_a in the range 0.2–0.3 μm (consistent with the target), except for steel D, whose specimens exhibited $R_a = 0.5$ μm. At the same time, the maximum roughness R_{max} ranged between 1.3 and 1.8 μm for all the steels except for steel D, which exhibited $R_{max} = 3.3$ μm. Despite the small differences of R_a, the topography of notch surfaces produced significantly different results between steel D ($R_a = 0.5$ μm) and the remaining ($R_a = 0.2$–0.3 μm), as suggested by the images in Figure 3A,B, acquired through the 3-D digital microscope Hirox KH-7700. As can be noted, numerous defects on both the notch-tip and notch-flank surfaces were detected

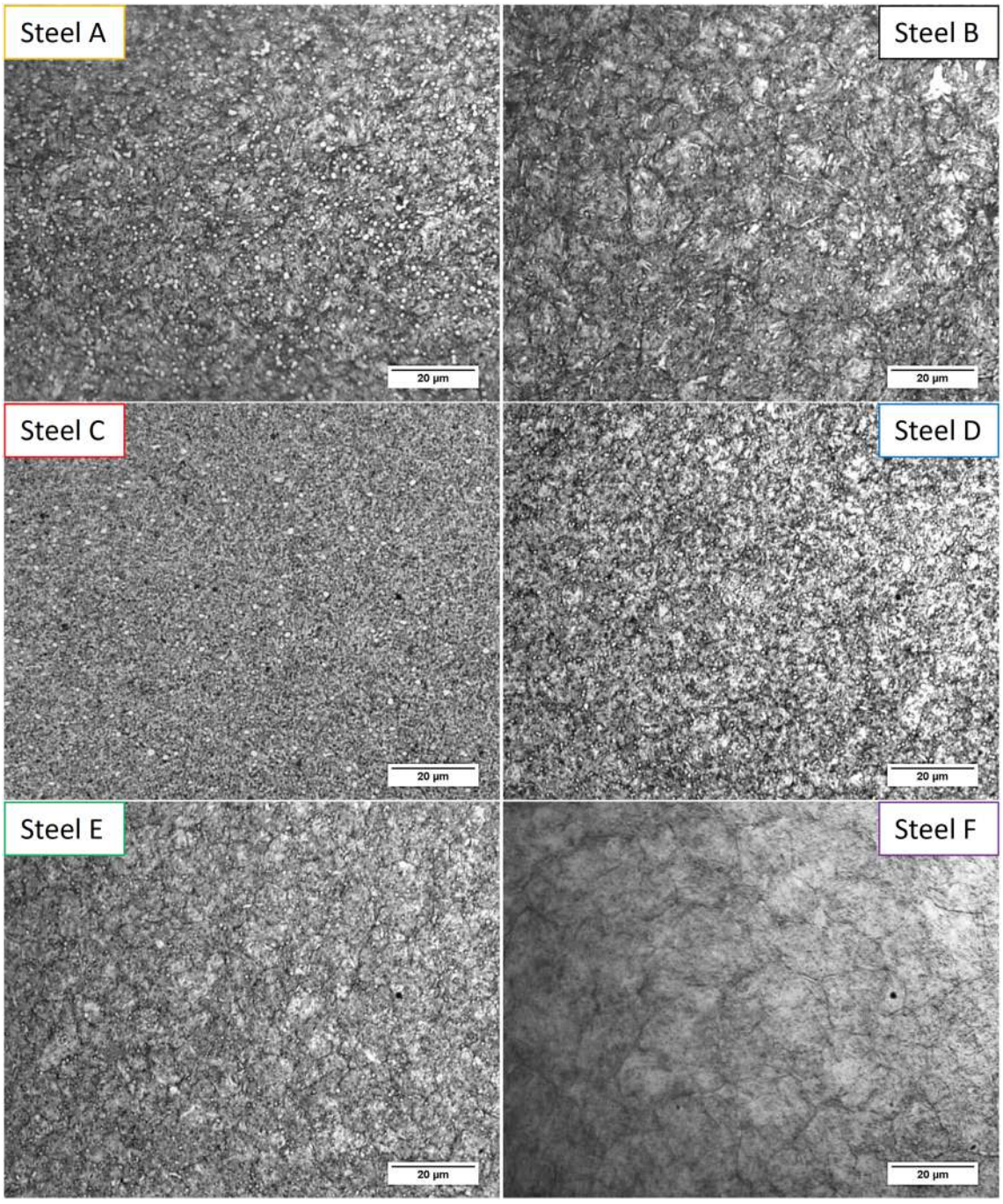

FIGURE 1 Microstructures of the investigated steels after heat treatment. OM images obtained on cross-sections polished and etched with 2% HNO_3 in ethanol [Colour figure can be viewed at wileyonlinelibrary.com]

Steel	A	B	C	D	E	F
HV	869 ± 21	805 ± 12	837 ± 24	752 ± 14	821 ± 13	643 ± 11

TABLE 3 Vickers hardness (average value ± standard deviation) of the investigated tool steels

in steel D ($R_a = 0.5$ µm), attributed to an improper machining of the notch.

The surface residual stress σ_{res} was evaluated according to EN 13925[52] using a GNR Stress-X X-ray diffractometer (Cr-Kα radiation with V filter, Ω scanning geometry, diffraction angle ψ scanned between −40° and 40°, 30 s of acquisition time on each position, (211) diffraction plane of α-Fe. No surface preparation performed.

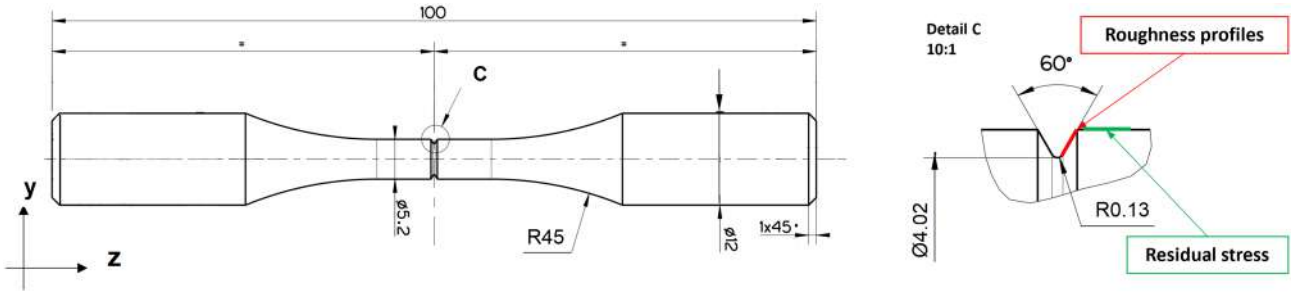

FIGURE 2 Geometry and dimensions (in mm) of the notched fatigue specimens. Detail C depicts the position and direction of evaluation of roughness profiles (in red) and residual stresses (in green) [Colour figure can be viewed at wileyonlinelibrary.com]

TABLE 4 Summary of average (R_a) and maximum (R_{max}) roughness (average value ± standard deviation) evaluated on the notch-flank of fatigue specimens

Steel	A	B	C	D	E	F
R_a (μm)	0.2 ± 0.0	0.2 ± 0.1	0.3 ± 0.1	0.5 ± 0.1	0.2 ± 0.0	0.3 ± 0.1
R_{max} (μm)	1.3 ± 0.3	1.8 ± 0.4	1.5 ± 0.4	3.3 ± 0.9	1.3 ± 0.4	1.8 ± 0.4

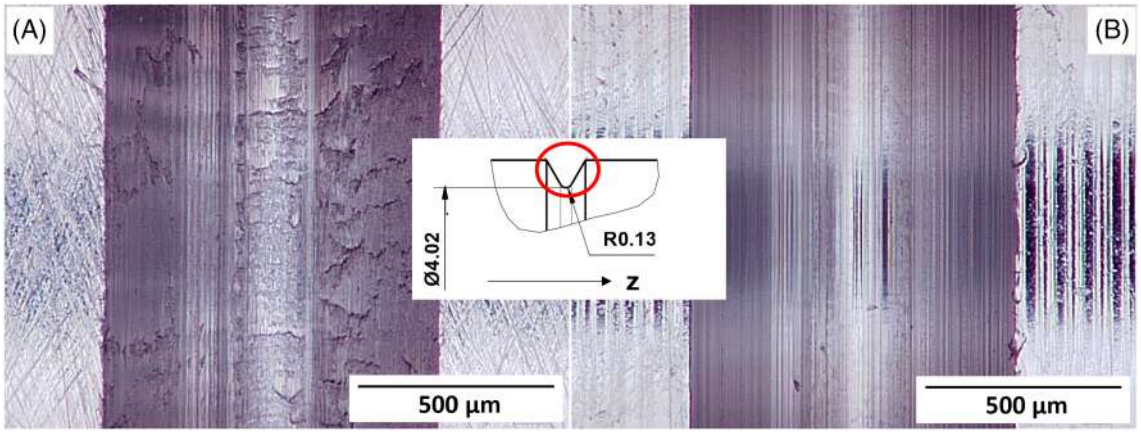

FIGURE 3 Appearance of the notch surface observed at the 3-D digital microscope: (A) steel D (R_a = 0.5 μm) and (B) steel E (R_a = 0.2 μm), representative of all investigated steels except for steel D [Colour figure can be viewed at wileyonlinelibrary.com]

TABLE 5 Summary of residual stress σ_{res} (average value ± standard deviation) evaluated on fatigue specimens

Steel	A	B	C	D	E	F
σ_{res}	−890 ± 73	−775 ± 39	−659 ± 61	−664 ± 95	−766 ± 103	−460 ± 102

Residual stress calculated according to sin2Φ method using the following elastic constants: $\nu = 0.293$, E = 211.4 GPa.) along the z direction, corresponding to the stress direction during fatigue tests. As for the roughness profiles, the available equipment did not allow residual stress measurements to be made on the notch-tip surface. Hence, σ_{res} was evaluated on the gage surface (5.2 mm diameter) very close to the notch, as indicated in Figure 2 (solid green line). It was assumed that the residual stress in this position is representative of the residual stress at the notch-tip. The summary of σ_{res} values (average value and standard deviation) is reported in Table 5. Negative values indicate compressive residual stresses. As can be noted, all the investigated steels exhibited strong compressive residual stresses, resulting from the machining operation.

The results of fatigue tests are shown graphically in the S-N diagram in Figure 4 (stress amplitude S against load cycles N). For each tool steel studied, Table 6 reports the corresponding notch fatigue strength at 10^7 cycles and 50% probability of failure, $L_{f,50\%}$, calculated according to ISO12107.[7] As can be noted, the investigated steels exhibited notch fatigue strengths $L_{f,50\%}$ ranging between 450 MPa (steel F) and 736 MPa (steel A) and can be

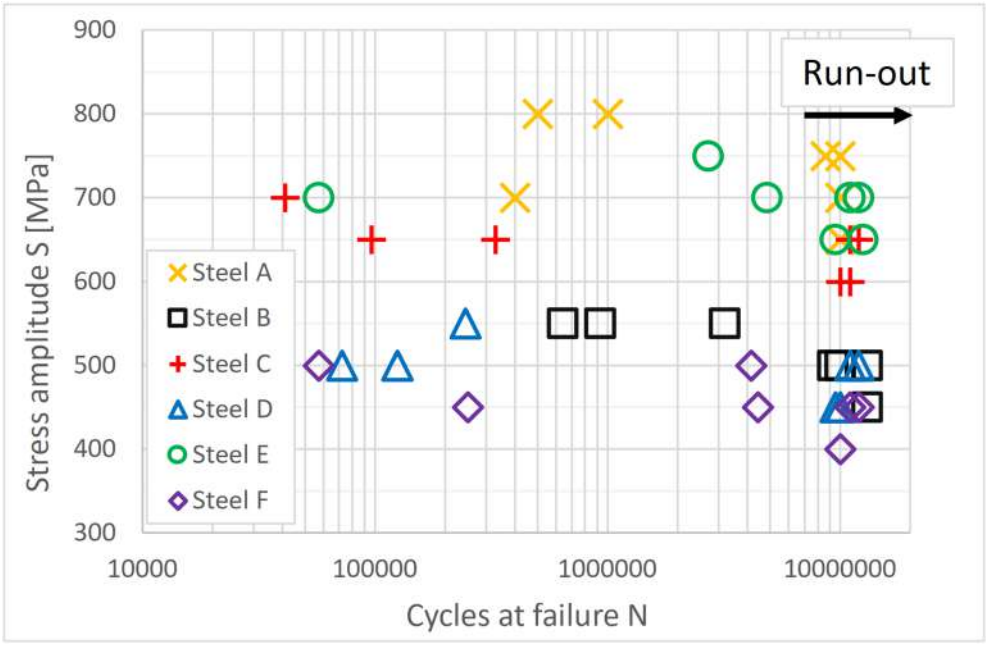

FIGURE 4 S-N data resulting from the notch fatigue tests [Colour figure can be viewed at wileyonlinelibrary.com]

TABLE 6 Summary of 10^7 cycles notch fatigue strength $L_{f,50\%}$ for the investigated tool steels

Steel	A	B	C	D	E	F
$L_{f,50\%}$ (MPa)	736	514	643	493	693	450

subdivided into two groups, "*high* $L_{f,50\%}$" (steels A, C, E) and "*low* $L_{f,50\%}$" (steels B, D, F).

Fracture surfaces of all the failed specimens were investigated by a scanning electron microscope (SEM, Zeiss EVO50) to determine the nucleation sites. The analysis of fracture surfaces suggested the effect of surface defects on the fatigue failures. In fact, in all the failed specimens of steel D ($R_a = 0.5$ μm, $R_{max} = 3.3$ μm), fatigue failures originated from overlapped surface defects at the notch-tip surface, as shown in Figure 5A, consistent with the defects attributed to improper notch machining shown in Figure 3A. The same fracture appearance was observed for some of the failed specimens of steel F (Figure 5B), despite the lower roughness measured on the notch-flank surface ($R_a = 0.3$ μm, $R_{max} = 1.8$ μm). In contrast, in the case of the "*high* $L_{f,50\%}$" steels (A, C, E), which also exhibited the lowest notch-surface roughness, crack nucleation was identified at the notch-tip surface, but no appreciable surface defect was clearly observed by SEM. However, it is worth noting that the fracture surfaces of several failed specimens of "*high* $L_{f,50\%}$" steels were dramatically affected by the damage resulting from the collision and sliding between the two half specimens after the fracture, which probably hid the actual fracture origin. None of the microstructural defects typically observed at the crack initiation sites of unnotched tool steels (non-metallic inclusions, large carbides, carbide clusters) was observed on the fracture surfaces of the investigated steels at fracture origin. The absence of these microstructural defects at the fracture origin can be explained by considering the stress field resulting from the rotating bending test and the severe notch, which produce an extremely high stress concentrated exclusively in a small volume of material close to the notch-tip surface.[9,10,15,17,32] Moreover, the innovative PM and ESR production processes result in steels with extremely high microstructural cleanliness, characterized by an overall low number of small non-metallic inclusions and uniform distributions of fine alloying carbides, with no carbide clusters, as shown in Figure 1. The combination of high stress concentration and microstructural cleanliness led to a low probability that a detrimental microstructural defect exists in the highly stressed volume at the notch-tip, and then to the predominant effect of surface conditions on the notch fatigue strength of the investigated tool steels.

In Figure 6, the experimental values of $L_{f,50\%}$ were plotted against the previously reported *HV* (Figure 6A), σ_{res} (Figure 6B), R_a (Figure 6C), and R_{max} (Figure 6D). The comparison indicated that the experimental notch fatigue strength $L_{f,50\%}$ of the six tool steels tested was certainly affected by steel hardness, surface finishing and residual stress. In particular, the steels which exhibited the highest $L_{f,50\%}$ ("*high* $L_{f,50\%}$" steels, A, C, E), were also characterized by the highest hardness *HV*, the lowest roughness (especially in terms of R_{max}) and a medium-to-high value of compressive residual stress σ_{res}. Steel A, which exhibited the overall highest $L_{f,50\%}$, also exhibited

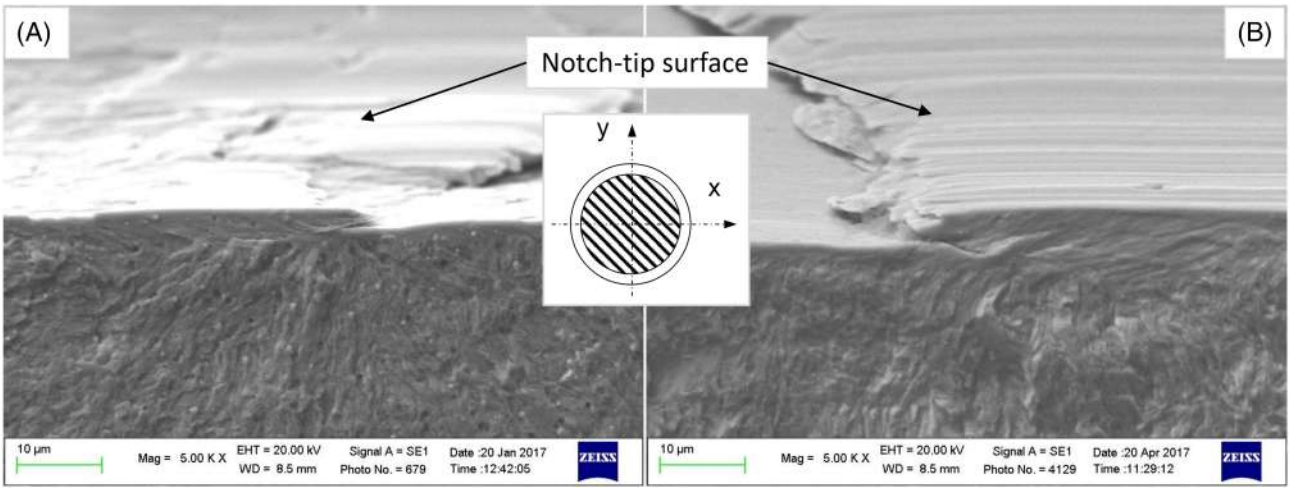

FIGURE 5 Representative SEM images of fracture surfaces of steel D (Figure 3A) and F (Figure 3B), showing the surface defects related to machining operations at the crack nucleation site [Colour figure can be viewed at wileyonlinelibrary.com]

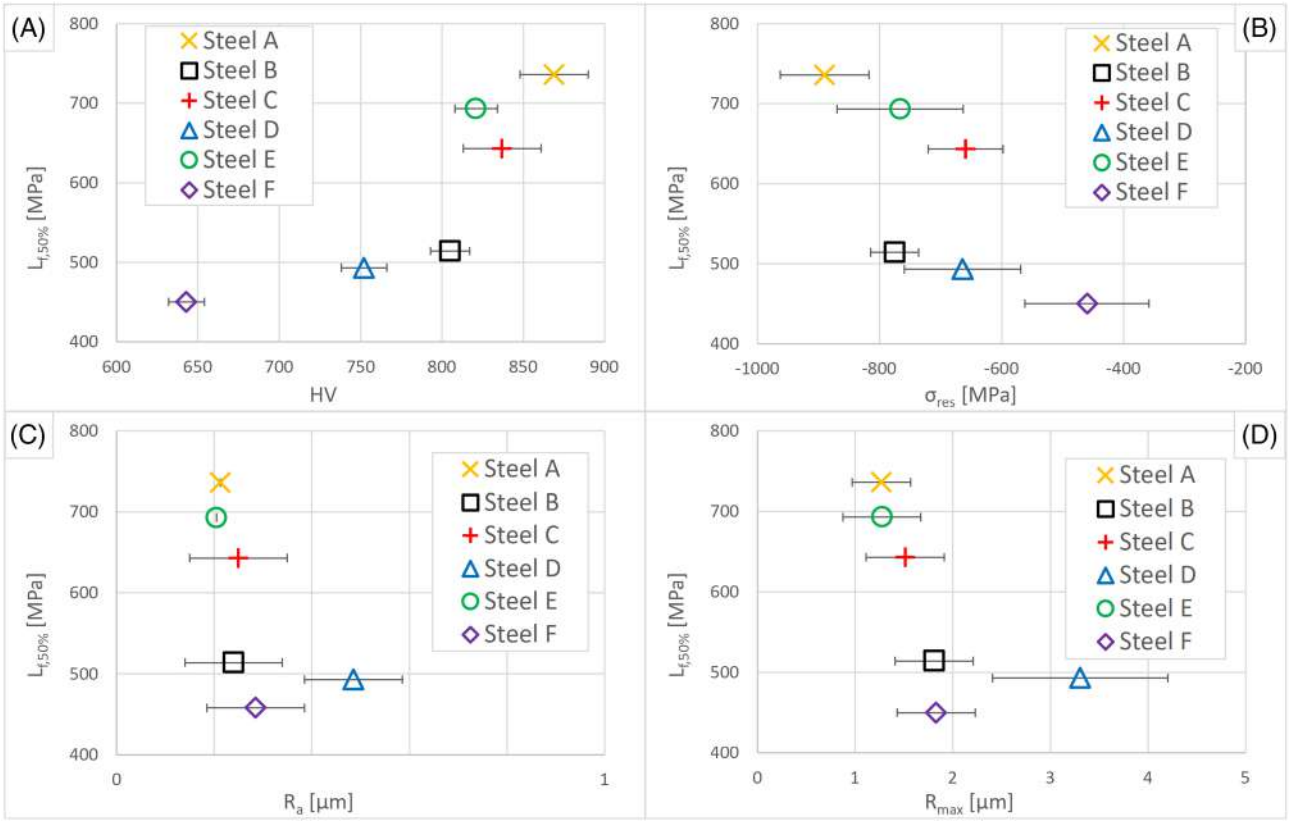

FIGURE 6 Experimental values of $L_{f,50\%}$ plotted vs. hardness HV (A), residual stress σ_{res} (B), average roughness R_a (C) and maximum roughness R_{max} (D) for the investigated steels [Colour figure can be viewed at wileyonlinelibrary.com]

the highest HV and σ_{res} and the lowest R_{max} among the investigated steels. Since steels A, C, E exhibited extremely similar values of R_a and R_{max}, the different $L_{f,50\%}$ was possibly due to different values of HV and σ_{res}. In contrast, the identification of clear trends between HV, σ_{res}, R_a, R_{max}, and $L_{f,50\%}$ for the "*low* $L_{f,50\%}$" steels (B, D, F) appeared more difficult. Steel F, which exhibited the lowest fatigue strength, was also characterized by the lowest HV and σ_{res}, but by roughness values similar to the "*high* $L_{f,50\%}$" specimens. In contrast, the low fatigue strength of steel D was attributed to the poor finishing of the notch surfaces ($R_a = 0.5$ µm, $R_{max} = 3.3$ µm), despite

a residual stress σ_{res} similar to the "*high* $L_{f,50\%}$" steels and hardness value *HV* intermediate between all the investigated steels. The fracture surfaces in Figure 5 and the analysis summarized in Figure 6 indicated that, beside steel hardness and surface residual stress, surface finishing plays a key role in determining the notch fatigue strength of the six tested tool steels, even in the considered low range of roughness.

3 | PROPOSED MODEL

A model for the prediction of high cycle notch fatigue strength of tool steels was developed, based on the experimental results in Section 2 and previous literature studies.[10,12,15,17,25–27,32,45,46] The main assumption of the model proposed in the present work is that surface finishing has a key role in the high cycle fatigue failure of notched tool steels, since fatigue cracks originate from the notch-tip surface.[10,15,17,25,26,53] In this model, all the valleys of the surface profile (assessed as the portion of the roughness profile below the mean line, as defined in ISO4287[54] and shown in Figure 7A), were considered as "surface defects" potentially responsible for notch fatigue failure disregarding their origin (machining marks, scratches, roughness valleys, etc.). Hence, in the following, the term "surface defects" will refer to the valleys indicated in Figure 7A.

According to the *square root of projected area* model proposed by Murakami[10] based on the projected area of defects, microstructural defects (like non-metallic inclusions and large carbides) and surface defects (including roughness valleys) can be considered as cracks of a given *area* (measured on the maximum stress plane, as described in Figure 7B), thus enabling the use of linear-elastic fracture mechanics (LEFM). Following LEFM, the local crack-tip stress field under cyclic loading conditions can be described by the stress-intensity factor range ΔK, which is related to the applied stress range $\Delta\sigma$ as well as to the size and position of the crack.[10,11,30,55] The *square root of projected area* model has been successfully adopted to describe the effect of different kinds of defects on fatigue failures in various materials, such as non-metallic inclusions in high strength and tool steels,[10,14,20,56] solidification defects in ductile irons,[57] geometric defects in Ti-6Al-4 V[58] and process-related and surface defects in parts produced by *Additive Manufacturing*.[46,59,60] Following the *square root of projected area* model, the stress-intensity factor range ΔK for a surface defect of a given *area* can be expressed by[10]:

$$\Delta K = 0.65 \cdot \Delta\sigma \cdot \sqrt{\pi \cdot \sqrt{area}} \tag{1}$$

where the coefficient 0.65 refers to surface defects and $\sqrt{area}$ represents the defect size parameter, without taking into account the defect shape, as proposed by Murakami[10] and described in Figure 7B. According to previous studies,[10,61–63] the high cycle fatigue strength (or, in case of most steels, the conventional *fatigue limit* at 10^7 cycles, if the fatigue behavior at higher number of cycles is disregarded) must be intended as the threshold stress for crack propagation, thus allowing the use of LEFM. LEFM relates ΔK to the crack growth rate. For a ΔK below a characteristic threshold value, namely, ΔK_{th}, the rate of crack growth is negligible, while for $\Delta K > \Delta K_{th}$ crack propagation occurs. ΔK_{th} represents the threshold condition for crack propagation and it is thus called

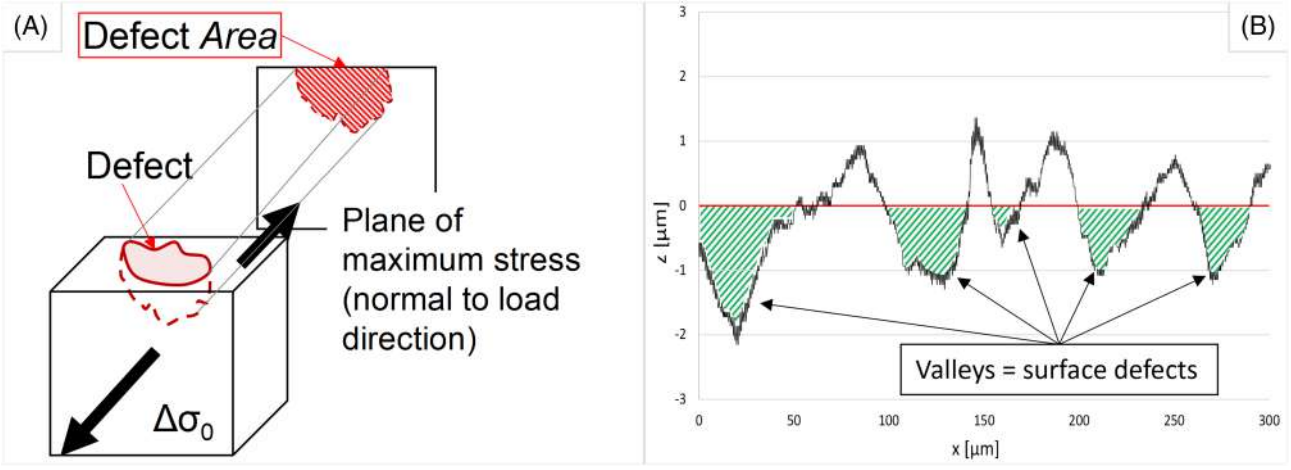

FIGURE 7 Example of surface roughness profile. In the present work, the valleys of the surface roughness profile (filled in green) are considered as surface defects (A). Schematic representation of defect *area* according to the *square root of projected area* model proposed by Murakami[10] (B) [Colour figure can be viewed at wileyonlinelibrary.com]

fatigue threshold. If, under an applied cyclic stress, the ΔK related to a crack exceeds the fatigue threshold ΔK_{th}, crack propagation occurs causing component failure within a finite number of load cycles.[10,30,61,63,64] Following these considerations, in the present work the 10^7 cycles fatigue strength was related to ΔK_{th} through LEFM. The onset of crack propagation ($\Delta K = \Delta K_{th}$) from surface defects, as previously defined, was considered the threshold condition for 10^7 cycles fatigue failures of notched tool steels. Therefore, a surface defect responsible for $\Delta K > \Delta K_{th}$ was considered as a *critical defect*.

In order to simulate the scatter of fatigue strength, a probabilistic approach for fatigue strength prediction was implemented following the model proposed by Meurling et al.,[12,45] which focuses on the key role of non-metallic inclusions and large carbides as crack initiation sites in high cycle fatigue failures of unnotched tool steels. However, the model proposed in the present work focuses on surface defects, as they were considered the dominant crack initiation sites in high cycle fatigue failures of notched tool steel components. In fact, as shown in Section 2, the effect of microstructural defects (non-metallic inclusions and large carbides) on the fatigue strength of notched components can be disregarded as a result of both the stress-concentration effect due to the notch[9,10,15,17,32] and the stress conditions associated with a rotating bending fatigue test, which determine the maximum stress in a very low surface volume. Moreover, the microstructural cleanliness resulting from the innovative ESR and PM production processes, used for manufacturing the considered tool steels, determines a low probability that a detrimental inclusion or a large carbide exists in the highly stressed volume at the notch-tip. Previous literature works has focused on the effect of defects on the fatigue strength.[12,45,59,60,65–68] Much research has sought to predict the greatest defect existing within a given volume, which is considered to be the most detrimental to fatigue strength, frequently by implementing a *largest extreme value distribution*.[59,60,65–68] However, following the work of Meurling et al.,[12,45] in the present work the fatigue strength prediction was not based on the maximum defect (i.e., the greatest carbide or inclusion in previous studies,[12,45] the deepest surface defect in the present work) but on the number of *critical defects* existing in the highly stressed region (on the notch-tip surface, were the greatest stress is achieved), that is, surface defects with $\Delta K > \Delta K_{th}$ and therefore potentially responsible for fatigue failures within a finite number of load cycles. This assumption allowed to introduce the probability of failure P_f (i.e., the probability that a specimen fails under an applied cyclic stress within a certain number of cycles, in this case 10^7) and thus to compute a distribution of fatigue strength (fatigue strength as a function of the probability of failure P_f). From this distribution, the fatigue strength can be calculated for different values of P_f (for example 50%). According to previous studies,[12,45] the probability of failure P_f can be related to the expected number of critical defects, λ_c, through a Poisson's distribution:

$$P_f = 1 - e^{-\lambda_c} \tag{2}$$

In the present work, λ_c was computed as the expected number of critical surface defects existing on the notch-tip surface along the circumferential direction by the equation:

$$\lambda_c = \pi \cdot d_{notch} \cdot N_{L(\sqrt{area}_c)} \tag{3}$$

where $\sqrt{area}_c$ represents the critical size parameter for propagation, $N_{L(\sqrt{area}_c)}$ the number of critical surface defects (with a size parameter $\sqrt{area} \geq \sqrt{area}_c$) per unit length, and d_{notch} the diameter of the notch-tip section (4.02 mm in the fatigue specimens shown in Figure 2). The size distribution of surface defects $N_{L(x)}$, defined as the number per unit length of surface defects with a size-parameter $\sqrt{area}$ higher than an arbitrary size x, was modelled as a two-parameter exponential-type function, following the model proposed in previous studies[12,45]:

$$N_{L(x)} = f \cdot e^{-k \cdot x} \tag{4}$$

An example of the $N_{L(x)}$ function, obtained from the experimental roughness profiles acquired on steel C in Section 2, is shown in Figure 8. The procedure that allows to compute the experimental points $(x; \sqrt{area})$ shown in Figure 8, and thus the $N_{L(x)}$ function, starting from the roughness profiles experimentally acquired in Section 2 will be thoroughly described in Section 4. $N_{L(x)}$ accounts for all the surface defects detected from the roughness profiles, as previously defined, despite their origin. According to the definition of $N_{L(x)}$ in Equation 4, f (mm^{-1}) represents the total number of surface defects per unit length (intersection between $N_{L(x)}$ and the vertical axis in Figure 8) and k (μm^{-1}) the slope of $N_{L(x)}$ on a semi-logarithmic plot, that is, the rate of decrease of $N_{L(x)}$ for increasing x.

Considering fatigue failures at 10^7 cycles, the critical size parameter for crack propagation $\sqrt{area}_c$ was computed introducing the fatigue threshold ΔK_{th} and the effective stress range $\Delta\sigma_{eff}$ in Equation 1:

$$\sqrt{area}_c = \frac{1}{\pi} \cdot \left(\frac{\Delta K_{th}}{0.65 \cdot \Delta\sigma_{eff}} \right)^2 \tag{5}$$

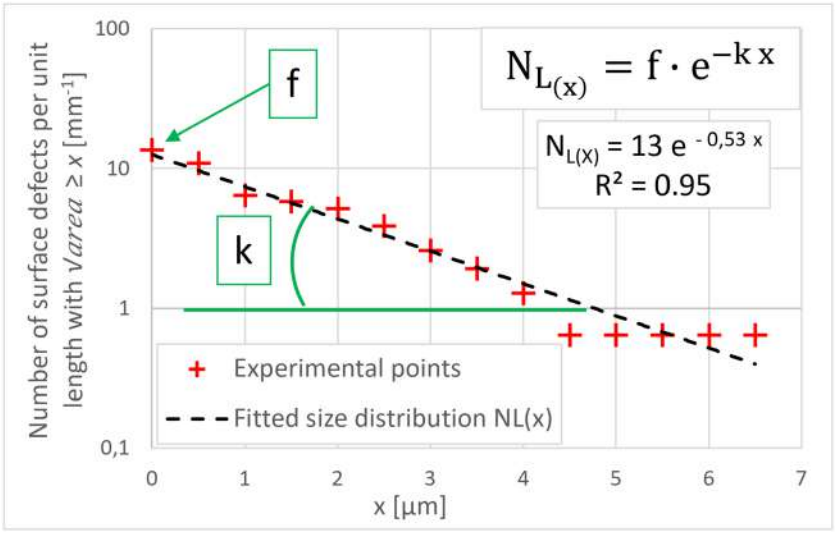

FIGURE 8 Example of the size distribution of surface defects $N_{L(x)}$, experimentally determined for steel C [Colour figure can be viewed at wileyonlinelibrary.com]

Following the work in previous studies,[12,45] in the present work, no interaction between contiguous defects was considered in the application of Equation 5. Although in previous studies[12,45] the fatigue threshold ΔK_{th} for tool steels was assumed equal to 4 MPa·m$^{1/2}$ (fatigue cracks initiated from non-metallic inclusion or carbides under a stress ratio R = 0.05), in the present work, a linear relationship between ΔK_{th} and the Vickers hardness HV was introduced, following existing relationships in the literature for estimating the fatigue threshold in high strength steels[10,69]:

$$\Delta K_{th} = 3.3 \cdot 10^{-3} \cdot HV + Z \tag{6}$$

where the constant Z was intended as the calibration parameter of the model. The model-calibration procedure to determine Z will be described in Section 4. The fatigue threshold ΔK_{th} estimated through Equation 6 and used in Equation 5 refers to short cracks under a stress ratio R = −1 (i.e., rotating bending or tension-compression fatigue tests with mean stress equal to zero). In fact, it must be considered that ΔK_{th} depends on both loading conditions (in particular on the stress ratio R) and crack length (in the present work represented by the size parameter $\sqrt{area}$). According to previous studies,[10,61,64,70–72] ΔK_{th} for short cracks is lower than for long cracks, meaning that a short crack can propagate for a ΔK below the ΔK_{th} of long cracks, due to incomplete crack closure. The formula for ΔK_{th} estimation proposed by Murakami,[10] on which Equation 6 is based, applies to short cracks and is effective up to a size $\sqrt{area}$ of approximatively 1000 μm. As will be shown in Section 4, the surface defects considered in the present work exhibited a maximum $\sqrt{area}$ below 15 μm; hence, they can be considered as short cracks. Considering the effect of the stress ratio R, the formula in Murakami,[10] on which Equation 6 is based, applies to a stress ratio R = −1. Moreover, during the experimental activity carried out in the present work only rotating bending fatigue tests (nominal stress ratio R = −1) were performed, as shown in Section 2; hence, no explicit relationship between stress ratio R and fatigue threshold ΔK_{th} was introduced.

The effective stress range $\Delta\sigma_{eff}$ was defined to describe the surface stress conditions induced by a rotating bending fatigue test (nominal stress ratio $R = -1$) in the presence of residual stress. Considering the crack propagation mode I,[55] only the tensile fraction of the stress cycle was considered for fatigue failures.[12] $\Delta\sigma_{eff}$ was computed as follows:

$$\begin{cases} \Delta\sigma_{eff} = \sigma_{max}\text{-}\sigma_{min} & \text{for } \sigma_{max} > 0 \text{ and } \sigma_{min} > 0 \\ \Delta\sigma_{eff} = \sigma_{max} & \text{for } \sigma_{min} \le 0 \\ \Delta\sigma_{eff} = 0 & \text{for } \sigma_{max} \le 0 \end{cases} \tag{7}$$

where σ_{max} and σ_{min} represent the maximum and minimum stresses along the loading direction at the notch-tip surface. σ_{max} and σ_{min} account for the stress concentration effect related to the notch and the surface residual stress σ_{res} along the loading direction. In the present work, the effect of a notch is considered to be fully represented by the theoretical stress concentration factor K_t. Hence, the proposed model is not suitable for sharp notches or, in general, notches with high acuity, even though it is not possible to indicate in advance a limiting value of acuity for the application of the proposed model. Conversely, the model is not suitable for un-notched tool steels ($K_t = 1$), since in this case fatigue failures initiate from microstructural defects.[9,10,22,25,26,12–14,16–20] However, it is not possible to indicate in advance a precise range of K_t for which the proposed model is suitable. As will be shown in Section 4, the model was validated for $K_t = 3$ so, in absence of further investigations, this can be considered as the maximum value of K_t for which the

model is valid. Moreover, steel hardness *HV* and residual stress σ_{res} were considered as two distinct and independent variables, and thus no explicit relationship between them was introduced, despite the fact that it is known that σ_{res} is generally proportional to steel hardness and yield strength. This assumption was made in order to consider the effect of different possible surface treatments and machining operations on σ_{res}, and hence on fatigue strength, even for the same values of steel hardness and yield strength. In fact, different surface residual stresses σ_{res} can be obtained in steel subjected to a specific heat treatment and therefore characterized by a defined hardness, by performing (or not) a shot peening surface treatment or by varying the peening parameters, as well as by using different surface finishing. Considering the stress concentration factor K_t and the residual stress σ_{res}, the maximum and minimum stresses along the load direction over the load cycle at the notch-tip surface, σ_{max} and σ_{min}, were defined as follows:

$$\sigma_{max} = +K_t \cdot \sigma_{nom} + \sigma_{res} \tag{8}$$

$$\sigma_{min} = -K_t \cdot \sigma_{nom} + \sigma_{res} \tag{9}$$

where σ_{nom} represents the nominal stress amplitude applied in a rotating bending fatigue test, and in the present work constitutes the independent variable for fatigue strength calculations.

To summarize, the developed model requires the following input variables to perform fatigue strength calculations: K_t (representative of notch severity), d_{notch} (mm) (representative of specimen size), *HV* (representative of steel hardness and thus mechanical strength), σ_{res} (MPa) (representative of surface residual stress), f (mm^{-1}) and k (μm^{-1}), which describe the size distribution of surface defects potentially responsible for fatigue failures. Through the previously reported equations (from Equation 2 to Equation 9), the probability of failure P_f associated with surface defects was computed as a function of the nominal stress-amplitude σ_{nom}; hence, $P_f = P_{f(\sigma_{nom})}$. The value of σ_{nom} which determines $P_f = 0.5$ was then considered as the 10^7 cycles notch fatigue strength at 50% probability of failure, namely, $L_{f,50\%}$. The above-mentioned system of equations was numerically solved through a dedicated MATLAB® script.

4 | MODEL VALIDATION AND ASSESSMENT OF PREDICTION ACCURACY

In order to assess the model effectiveness in fatigue strength prediction of notched tool steels, the experimental data collected in Section 2, including hardness and surface residual stress data reported in Table 3 and Table 5 and the roughness profiles from which the average and maximum roughness R_a and R_{max} reported in Table 4 were calculated, were used as model input to calculate the 10^7 cycles notch fatigue strength at 50% probability of failure, $L_{f,50\%}$, for the investigated tool steels. The input parameters d_{notch} and K_t were set equal to $d_{notch} = 4.02$ mm and $K_t = 3$ for all the considered steels, in order to simulate the notch-tip diameter and the theoretical stress-concentration factor of the specimens used for the fatigue tests (Figure 2). For each steel, the remaining input parameters required for fatigue strength calculation using the developed model, f and k, representative of the size distributions of surface defects $N_{L(x)}$ (an example of which is shown in Figure 8), were calculated by processing the roughness profiles experimentally acquired on the notch-flank surfaces of the fatigue specimens (previously described in Section 2) using a dedicated MATLAB® script. Due to impossibility to perform roughness measurements on the notch-tip surface along the circumferential direction, the roughness profile on the notch-flank surface along the z direction was assumed to be representative of the one on the notch-tip surface along the circumferential direction. Similarly, the surface residual stress σ_{res} evaluated close to the notch, as highlighted in Figure 8, was assumed to be representative of the one on the notch-tip surface. Each roughness profile was processed using a MATLAB® script which detects surface defects (defined as shown in Figure 7A) and, for each defect, computes the size parameter $\sqrt{area}$. Then, surface defects were classified according to the size parameter $\sqrt{area}$. The size distribution of surface defects was obtained by plotting the number of surface defects per unit length with a size parameter $\sqrt{area}$ higher than an arbitrary size x as a function of x, as shown in Figure 8. By fitting the experimental points $(x; \sqrt{area})$ through a two-parameter exponential function (described by Equation 4), the size distribution of surface defects $N_{L(x)}$ was obtained, and thus the parameters f and k required for model calculations. This procedure was performed for each of the investigated steels; hence, a specific function $N_{L(x)}$ and different values of f and k were obtained for each steel. Figure 8 shows the points $(x; \sqrt{area})$ and the resulting function $N_{L(x)}$ obtained from the roughness profiles acquired on steel C. The results shown in Figure 8 are also qualitatively representative of the remaining steels, except for the numeric values of f and k.

Table 7 summarizes the values of f and k determined through the described procedure for the six notch tool steels experimentally investigated. Comparing the data in Table 4 (average and maximum roughness values R_a and

TABLE 7 Summary of f and k values, representative of the size distributions of surface defects $N_L(x)$, obtained from the roughness profiles of the tool steels experimentally investigated in Section 2

Steel	A	B	C	D	E	F
f (mm^{-1})	36	11	13	16	28	12
k (μm^{-1})	0.73	0.21	0.53	0.25	0.69	0.36

R_{max}) and Table 7 (f and k parameters representative of size distribution of surface defects $N_{L(x)}$), it can be noted that f and k strongly varied between the investigated steels despite the small difference of roughness (R_a and R_{max}) and even between steels with the same average roughness R_a. This evidence suggested that R_a is not representative of the distribution of surface defects and that roughness profiles with the same average roughness R_a can have different $N_{L(x)}$, thus different f and k. Moreover, the overall number per unit length of surface defects f ranged between 11 and 36 mm^{-1}, while k ranged between 0.21 and 0.73 μm^{-1}. It is worth noting that the steels characterized by the highest values of R_{max} ("*low* $L_{f,50\%}$" steels B, D, F) exhibited the lowest values of f and k parameters. Considering the definitions of $N_{L(x)}$ (Equation 4), the combination of low f and k can be intended as related to the presence of an overall low number of surface defects, but of large size. In comparison, steels with the lowest R_{max} ("*high* $L_{f,50\%}$" steels A, C, E) exhibited the highest f and k parameters, which can be associated to the presence of a high number of surface defects of a small size. However, the definition of clear trends between R_{max}, f and k requires further analyses.

In order to perform fatigue strength calculations through the proposed model, the determination of the calibration parameter "Z" in Equation 6 was required. Since the six steels experimentally tested in the present work exhibited similar characteristics, the parameter "Z" was intended as common among them. The calibration procedure was therefore performed only on a single set of input parameters representative of one of the six steels investigated. Following this aim, the model-calibration procedure was performed by iteratively calculating $L_{f,50\%}$ for steel C (input parameters: $d_{notch} = 4.02$ mm, $K_t = 3$, $HV = 837$, $\sigma_{res} = -659$ MPa, $f = 13$ mm^{-1}, $k = 0.53$ μm^{-1}) using different values of Z, with the target of minimizing the difference between model-predicted and experimental $L_{f,50\%}$. The value of Z which resulted in the minimum prediction error was then set as the model-calibration parameter Z in Equation 6. From this procedure, the value $Z = 1.9$ MPa·$m^{1/2}$ was obtained. Steel C was used for model calibration since it exhibited an intermediate experimental value of $L_{f,50\%}$ (643 MPa) amongst the tested steels. The value of $Z = 1.9$ MPa·$m^{1/2}$ determined through the described calibration procedure performed on steel C was then adopted for the fatigue strength calculations of all the remaining steels, without the reiteration of the calibration procedure (and thus the determination of a specific Z for each steel). It is worth noting that with $Z = 1.9$ MPa·$m^{1/2}$, Equation 6 predicted values of the fatigue threshold ΔK_{th} for the investigated tool steels ranging between 4 and 4.8 MPa·$m^{1/2}$, which is very close to the values of ΔK_{th} reported in literature for short cracks in tool steels (approximately 4–6 MPa·$m^{1/2}$ for a stress ratio $R = -1$).[13,14]

Figure 9A shows the comparison between the experimental $L_{f,50\%}$ for the investigated tool steels, determined in Section 2, and the predicted $L_{f,50\%}$ calculated through the developed model, using as input parameters the values of HV and σ_{res} listed in Table 3 and Table 5 respectively, f and k listed in Table 7, experimentally determined for each steel. The remaining input parameters d_{notch} and K_t and the calibration parameter Z were kept as constants amongst all the six steels, respectively, equal to $d_{notch} = 4.02$ mm and $K_t = 3$ (both representative of fatigue specimens used in the experimental fatigue tests, shown in Figure 2) and $Z = 1.9$ MPa·$m^{1/2}$ (determined on steel C, as previously described). This calculation was indicated as "calculation A". As can be noted, a very good agreement between model-predicted and experimental notch fatigue strength was found for the six tool steels investigated. The average and maximum prediction error was 1.3% and 3.1%, respectively. Obviously, steel C exhibited the lowest prediction error, since model calibration was performed on the dataset experimentally determined on steel C. However, no other calibration was made for the remaining steels, nor data fitting between the input parameters and $L_{f,50\%}$ (experimental and model-predicted), thus indicating the validity of $Z = 1.9$ MPa·$m^{1/2}$ for all the six investigated steels. These results suggest that the proposed model is effective in the prediction of the high cycle notch fatigue strength for tool steels with hardness in the range 640–870 HV. Moreover, the low prediction error obtained without iterating the calibration procedure for each steel investigated suggests that the developed model could potentially be applied to tool steels with similar characteristics. Figure 9A seems to confirm that surface finishing plays a dominant role in fatigue failures of notched tool steels, even in the low range considered of R_a (0.2–0.5 μm), strengthening the main assumption of the model that high cycle fatigue failures in notched tool steels originate from surface defects. This result can be explained by considering the data in Table 7, which show that the parameters f and k, used as input parameters for model calculations, exhibited greatly different values among the considered R_a range and even for the same R_a, indicating that different distributions of surface defects $N_{L(x)}$ are possible for

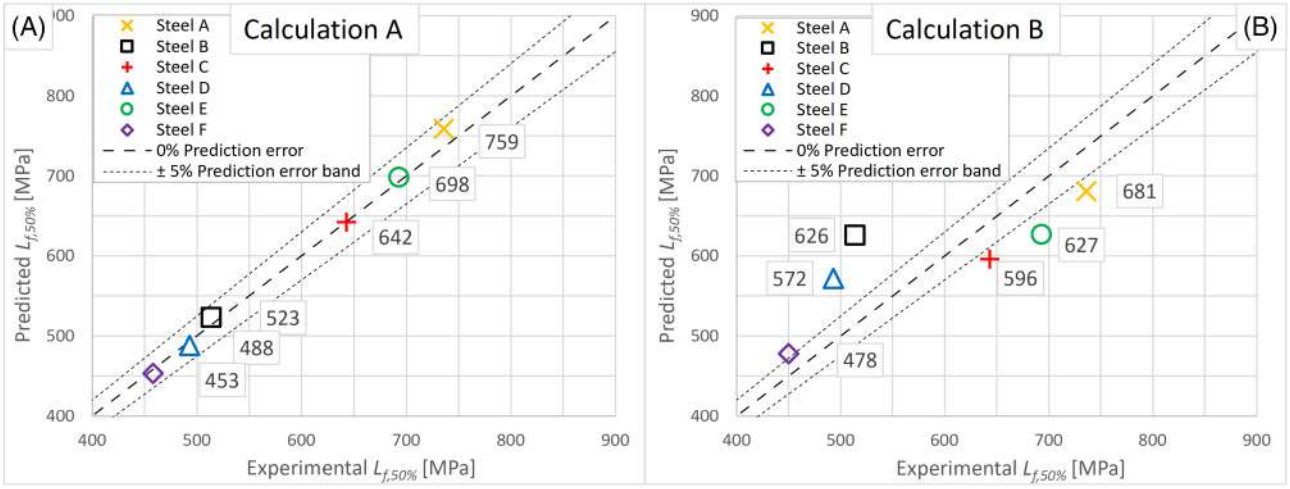

FIGURE 9 Comparison between experimental and model-predicted $L_{f,50\%}$ for the investigated tool steels considering (A) different f and k parameters for each steel (calculation A) and (B) common f and k parameters for all the steels [Colour figure can be viewed at wileyonlinelibrary.com]

the same R_a. Moreover, also the maximum roughness R_{max} can differ significantly at the same average roughness R_a. Therefore, R_a appears unsuitable to effectively describe the surface features which define the fatigue behavior of notched tool steels. In order to further investigate this hypothesis through the developed model, a second fatigue strength calculation was performed (hereafter indicated as "calculation B"), by assuming a different hypothesis that resulted in a different definition of f and k parameters. Calculation B was based on the assumption that, in the considered range of average roughness $R_a = 0.2$–0.5 μm, different distributions of surface defects $N_{L(x)}$ (thus different f and k) are not possible and surface finishing does not play a key-role in notch fatigue failures. Therefore, according to this assumption, in the range $R_a = 0.2$–0.5 μm $L_{f,50\%}$ is only affected by HV and σ_{res} (at a given specimen size and stress-concentration factor K_t), while the effect of different surface finishing is negligible. In order to perform $L_{f,50\%}$ calculations according to these new assumptions, all the roughness profiles acquired in Section 2 for the six tool steels were processed again through the previously described procedure, but with no distinction between the different steels. As a result, a single set of f and k parameters was obtained, respectively equal to $f = 22\ \text{mm}^{-1}$ and $k = 0.47\ \mu\text{m}^{-1}$, which were used as input parameters in calculation B for all the considered tool steels. To summarize, the main difference between calculation A and B is that in calculation A, the parameters representative of size distributions of surface defects, f and k, have different values for each steel, while in calculation B their value was constant for all the steels. For calculation B, $L_{f,50\%}$ was computed through the model using the values of HV and σ_{res} listed in Table 3 and Table 5 (different HV and σ_{res} for each steel). The remaining parameters were kept as constants amongst all the considered steels, respectively equal to $d_{notch} = 4.02$ mm, $K_t = 3$, $Z = 1.9$ MPa·m$^{1/2}$, $f = 22\ \text{mm}^{-1}$ and $k = 0.47\ \mu\text{m}^{-1}$. Figure 9B shows the comparison between the experimental $L_{f,50\%}$ for the investigated tool steels, determined in Section 2, and the predicted $L_{f,50\%}$ calculated according to calculation B. As can be noted, the assumption made in calculation B led to a considerably worst agreement between experimental and model-predicted $L_{f,50\%}$ values, with average and maximum prediction error respectively equal to 11.4% and 21.8%. This result further strengthens the hypothesis that $L_{f,50\%}$ is not only affected by HV and σ_{res}, but also by the distribution of surface defects, represented by f and k parameters, thus confirming the crucial effect of surface finishing on notch fatigue strength, even for average roughness values in the range $R_a = 0.2$–0.5 μm.

5 | ASSESSMENT OF MODEL BEHAVIOR

The dotted red line in Figure 10 shows an example of the model-predicted distribution of fatigue strength, represented as the probability of failure P_f as a function of the nominal stress-amplitude σ_{nom}, obtained with the following input parameters: $K_t = 3$, $d_{notch} = 4$ mm, $HV = 700$, $\sigma_{res} = -700$ MPa, $f = 25\ \text{mm}^{-1}$, $k = 0.4\ \mu\text{m}^{-1}$, Z = 1.9 MPa·m$^{1/2}$. Considering $P_{f(\sigma_{nom})}$ as the cumulative distribution of failure probability, the probability density function $PDF_{(\sigma_{nom})}$ related to $P_{f(\sigma_{nom})}$ can be obtained by deriving $P_{f(\sigma_{nom})}$ with respect to σ_{nom}:

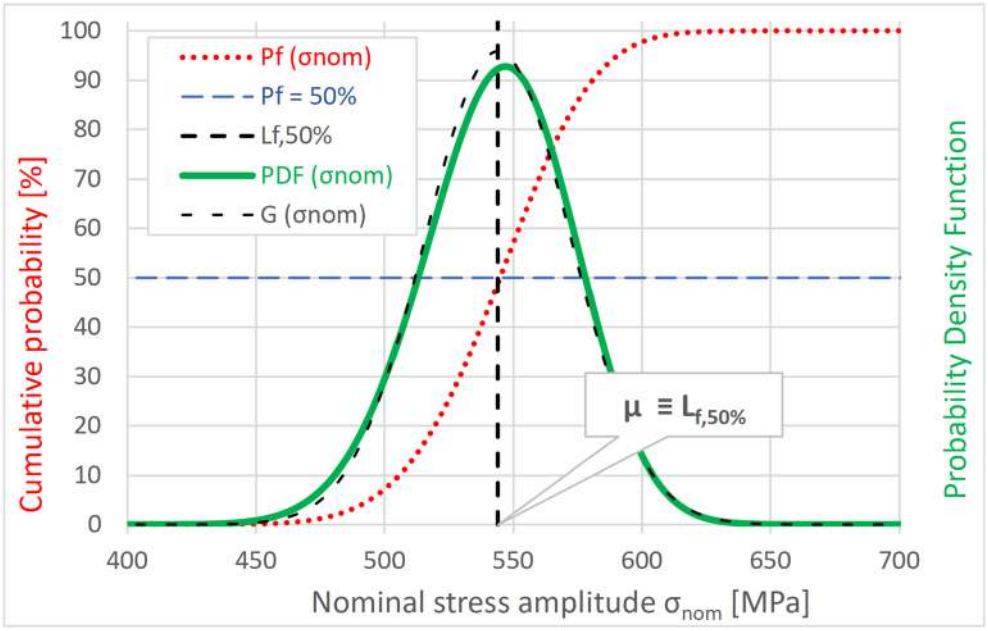

FIGURE 10 Example of failure probability P_f (dotted red line) and density function of failure probability *PDF* (solid green line) computed by the model as a function of σ_{nom}. The black dash-dot line represents the normal function $G_{(\sigma_{nom})}$ approximating *PDF*. Input parameters: $K_t = 3$, $d_{notch} = 4$ mm, $HV = 700$, $\sigma_{res} = -700$ MPa, $f = 25\ \text{mm}^{-1}$, $k = 0.4\ \mu\text{m}^{-1}$, $Z = 1.9\ \text{MPa}\cdot\text{m}^{1/2}$ [Colour figure can be viewed at wileyonlinelibrary.com]

$$PDF_{(\sigma_{nom})} = \frac{dP_{f(\sigma_{nom})}}{d\sigma_{nom}} \tag{10}$$

In Figure 10, $PDF_{(\sigma_{nom})}$ is represented by the solid green line. As can be noted, $PDF_{(\sigma_{nom})}$ can be fitted with good approximation by a normal function $G_{(\sigma_{nom})}$ with mean value μ and standard deviation *SD* given by the following equation:

$$G_{(\sigma_{nom})} = \frac{1}{SD \cdot \sqrt{2\pi}} e^{-\frac{1}{2}\left(\frac{\sigma_{nom}-\mu}{SD}\right)^2} \tag{11}$$

It is noticeable that the mean value μ of $G_{(\sigma_{nom})}$ roughly corresponds to the predicted notch fatigue strength at 50% probability of failure; hence, it can be considered $\mu = L_{f,50\%}$. According to ISO12107,[7] the fatigue strength at a given number of cycles is a random variable described by a normal distribution. Hence the developed model appears to be able to describe the variability of fatigue strength, since it predicts a normal distribution of fatigue strength. Note that, despite the distributions shown in Figure 10 were obtained using a specific set of input parameters, normal (or closely normal) distributions of fatigue strength were obtained over wide ranges of input parameters, and in particular for all the sets of input parameters determined through the experimental activity on the investigated steels and used for the calculations in Section 4. Moreover, even though a probabilistic approach was implemented through Equation 2 following the work in previous studies,[12,45] the fact that the distribution of failure probability $P_{f(\sigma_{nom})}$ follows a normal function was not explicitly modelled, but it independently arises from the equations which define the model itself (from Equation 2 to Equation 9). In order to quantify the model-predicted variability of fatigue strength, the following coefficient of variation *CV* was computed:

$$CV = \frac{SD}{L_{f,50\%}} \tag{12}$$

CV represents a measure of the relative scatter of the predicted fatigue strength distribution, since the higher *CV* is, the higher the variability of fatigue strength is. For the same $L_{f,50\%}$, a higher *CV* indicates a higher standard deviation *SD*, and hence a wider distribution.

In order to evaluate the model response (in terms of $L_{f,50\%}$ and *CV*) to variations of input parameters (K_t, d_{notch}, *HV*, σ_{res}, *f*, *k*), a sensitivity analysis was performed varying each input variable from its reference value, set as $K_t = 3$, $d_{notch} = 4$ mm, $HV = 700$, $\sigma_{res} = -700$ MPa, $f = 25\ \text{mm}^{-1}$, $k = 0.4\ \mu\text{m}^{-1}$. The calibration parameter Z in Equation 6 was assumed equal to $Z = 1.9\ \text{MPa}\cdot\text{m}^{1/2}$, determined by the procedure described in Section 4. The predicted effect of steel hardness *HV* on notch fatigue strength is shown in Figure 11A. As can be seen, an increase of *HV* leads straight to an improvement of $L_{f,50\%}$. This trend directly arises from the linear relationship between the hardness *HV* and the fatigue threshold ΔK_{th} established through Equation 6 and it is consistent with the literature data and experimental evidence. In fact, it is known from a previous study[10] that in metals with hardness ranging from 70 to 720 *HV*, a hardness increase results in higher fatigue threshold and strength. The *CV-HV* trend appeared roughly constant, since the variation of *CV* is approximatively 1% over the considered wide range of

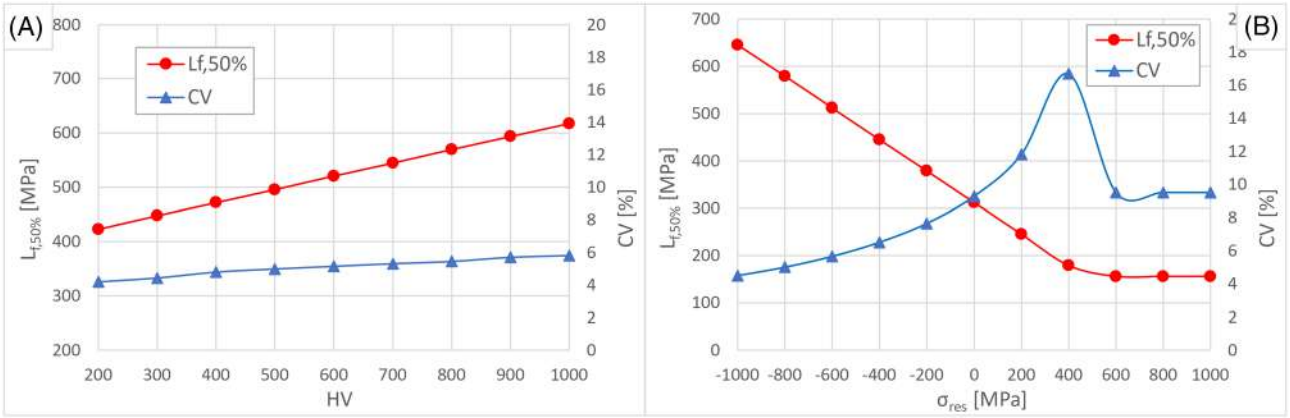

FIGURE 11 Effect of steel hardness *HV* (A) and surface residual stress σ_{res} (B) on predicted $L_{f,50\%}$ and *CV* [Colour figure can be viewed at wileyonlinelibrary.com]

HV. This evidence indicates that, according to the proposed model, the relative scatter of fatigue strength does not depend on steel hardness *HV*, meaning that for higher *HV* both $L_{f,50\%}$ and the standard deviation *SD* rise, but their ratio (*CV*) is constant.

Figure 11B shows the predicted effect of surface residual stress σ_{res}. For a compressive residual stress ($\sigma_{res} < 0$), a linear relationship between σ_{res} and $L_{f,50\%}$ exists, implying that the higher the compressive stress in surface layers, the higher the notch fatigue strength, as expected from the literature data.[33,73] The linear trend is maintained up to moderate tensile residual stresses ($\sigma_{res} > 0$), while for high tensile σ_{res} the model predicts a steady minimum value of fatigue strength $L_{f,50\%}$. The predicted trend of $L_{f,50\%}$ against σ_{res} arises from the set of equations which defines the effective stress range $\Delta\sigma_{eff}$ (from Equation 7 to Equation 9). For a compressive residual stress ($\sigma_{res} < 0$), the minimum stress over the load cycle σ_{min} is clearly negative, therefore the effective stress range $\Delta\sigma_{eff}$ only depends on σ_{max}. As the compressive residual stress increases (in absolute value), σ_{max} decreases so the effective stress range $\Delta\sigma_{eff}$ is reduced, resulting in an improved notch fatigue strength $L_{f,50\%}$. On the other hand, for a tensile residual stress ($\sigma_{res} > 0$), σ_{min} can be either negative or positive. In the latter case, $\Delta\sigma_{eff}$ is not affected by σ_{res} since both σ_{max} and σ_{min} equally depend on σ_{res}. Therefore, for a high tensile residual stress, the predicted notch fatigue strength $L_{f,50\%}$ is not affected by σ_{res}. The coefficient of variation *CV* exhibits a peak for the value of σ_{res} corresponding to the transition from linear to steady of the $L_{f,50\%}$-σ_{res} curve. It is worth noting that, starting from this point, *CV* monotonically decreases for increasing compressive residual stress ($\sigma_{res} < 0$), indicating a reduction in fatigue strength variability. Therefore, the proposed model predicts a beneficial effect of high surface compressive residual stress on fatigue behavior, since it results in both higher fatigue strength and lower scatter. It is also worth noting that high surface compressive residual stresses are generally introduced in engineering components through adequate treatments, such as shot peening, precisely to improve the fatigue behavior, as already pointed out.[33,73–75]

Figure 12 shows the effect of *f* and *k* parameters, representative of the size distribution of surface defects, and hence of surface finishing. As can be seen, *f* and *k* have opposite effects on notch fatigue strength. As *f* increases, $L_{f,50\%}$ is reduced toward an asymptotic minimum value (Figure 12A), while for increasing *k*, $L_{f,50\%}$ shows a great improvement (Figure 12B). Both the trends of $L_{f,50\%}$ against *f* and *k* can be explained considering the distribution of surface defects $N_{L(x)}$ modelled in the proposed model through Equation 4, in which *f* represents the total number per unit length of defects and *k* the rate of decrease of $N_{L(x)}$ for increasing *x*. Referring to Figure 8, as *f* increases $N_{L(x)}$ is shifted to higher values, while for reductions of *k* $N_{L(x)}$ approaches 0 at a lower rate (i.e., at higher *x*). In both cases, the number per unit length of surface defects with a great size parameter $\sqrt{area}$ increases and thus the expected number of critical defects existing on the notch-tip surface λ_c increases, resulting in the prediction of a lower notch fatigue strength $L_{f,50\%}$. Blue lines in Figure 12 indicate that the coefficient of variation *CV* roughly follows the trends of $L_{f,50\%}$ against *f* and *k*, even if the variations are within different ranges (between 4% and 12% for *CV*-*f* trend, between 4% and 6% for *CV*-*k* trend).

Figure 13A shows the model-predicted effect of notch-tip diameter d_{notch}, assumed to be representative of specimen size. As is evident from the solid red line, the predicted notch fatigue strength $L_{f,50\%}$ decreases as specimen size increases. This trend can be explained by considering Equation 3, where d_{notch} determines the length

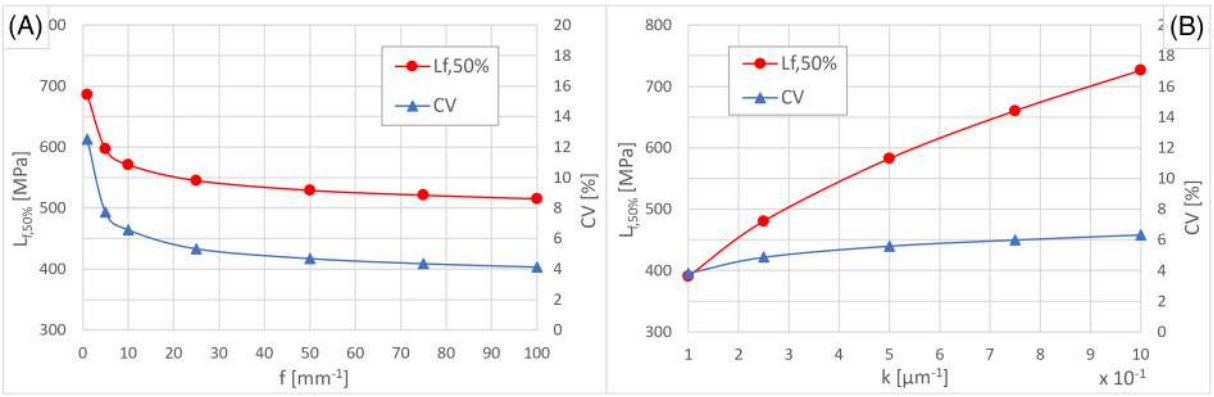

FIGURE 12 Effect of f (A) and k (B) parameters describing the size distribution of surface defects on predicted $L_{f,50\%}$ and CV [Colour figure can be viewed at wileyonlinelibrary.com]

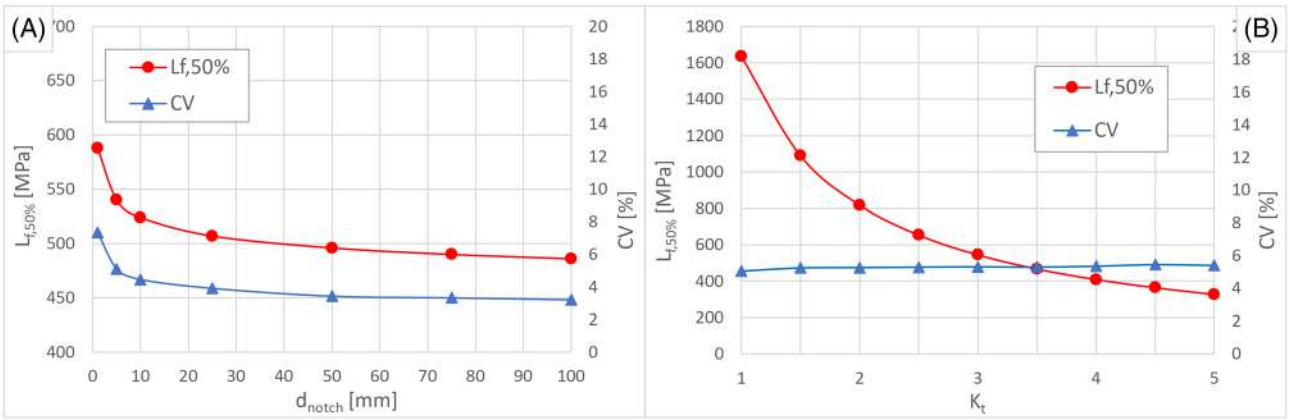

FIGURE 13 Effect of notch-tip diameter d_{notch} (A) and stress concentration factor K_t (B) on predicted $L_{f,50\%}$ and CV [Colour figure can be viewed at wileyonlinelibrary.com]

over which the expected number of critical surface defects λ_c is computed. For a given distribution of surface defects $N_{L(x)}$ (i.e., given f and k parameters), an increase in d_{notch} involves a higher number of critical defects λ_c and thus a lower predicted $L_{f,50\%}$. The trend is consistent with the size-dependent factors generally applied in machine design to reduce fatigue strength for increasing size.[11] The coefficient of variation CV roughly follows the trend of $L_{f,50\%}$ against d_{notch}. According to the proposed model both curves have higher steepness for lower specimen size d_{notch}. This suggests that both $L_{f,50\%}$ and the scatter of fatigue strength are greatly affected by specimen size for low d_{notch}, while they settle on minimum and approximately steady values for high values of d_{notch}.

Figure 13B shows the predicted effect of the theoretical stress concentration factor K_t, ranging between $K_t = 1$ (unnotched specimen) and $K_t = 5$ (severely notched specimen). As can be seen, as K_t increases $L_{f,50\%}$ is monotonically reduced, indicating the capability of the developed model to simulate the detrimental effect of stress raisers on fatigue strength. Note that the slope of the $L_{f,50\%}$-K_t curve decreases as K_t increases, indicating a lower sensitivity of $L_{f,50\%}$ on K_t, for increasing K_t. Since the variation of CV over the considered range of K_t is negligible, it can be considered that, according to the developed model, K_t does not affect the scatter of fatigue strength. Even though the sensitivity analysis was performed between $K_t = 1$ and $K_t = 5$, it must be considered that the developed model cannot probably be applied to unnotched tool steels ($K_t = 1$), since in that case fatigue failures typically initiate at sub-surface microstructural defects, such as non-metallic inclusions and carbides.[9,10,12–22] Similarly, it is not possible to indicate in advance the exact range of K_t on which the proposed model is valid.

The results shown in the present section indicated that the model is potentially effective in representing the scatter of fatigue strength, beside the calculation of fatigue strength at a given probability of failure (50%, in the case of $L_{f,50\%}$). Furthermore, the trends of model outputs ($L_{f,50\%}$ and CV) obtained by the sensitivity analysis

can be explained considering the relationships implemented in the model definition and appeared consistent with experimental and literature data.

6 | CONCLUSIONS AND FUTURE WORK

A model for notch fatigue strength prediction of high strength tool steels based on fracture mechanics was developed. The main assumption of the model is that surface defects (machining marks, scratches, and roughness valleys) existing at the notch tip are the root cause of notch fatigue failures of these steels for two main reasons: the high K_t due to the notch, which leads to high stresses only in a very low volume near to the notch-tip surface, and the low content of microstructural defects, such as non-metallic inclusions, resulting from the new ESR and PM production processes of these steels. The model also takes into account the effect of steel hardness, residual stress, notch severity and specimen size. Due to the implemented probabilistic approach, distributions of fatigue strength were predicted. The following conclusions can be drawn:

- The proposed model was effective in describing the scatter of fatigue strength by predicting normal distributions of fatigue strength, from which the 10^7 cycles notch fatigue strength at 50% probability of failure $L_{f,50\%}$ and the coefficient of variation CV, representative of fatigue scatter, were obtained.
- The model was validated on the data resulting from the experimental activity performed on six notched tool steels, produced by ESR and PM and heat treated to final hardness in the range 640–870 HV. Average and maximum error between the model-predicted and experimental notch fatigue strength was only 1.3% and 3.1%, respectively.
- The model was used to investigate the effect of surface finishing on fatigue strength in the considered range $R_a = 0.2$–0.5 μm. The results indicated that surface defects, and thus surface finishing, have a non-negligible effect on fatigue strength of notched tool steels even in the considered range of roughness.
- The sensitivity analysis indicated the model effectiveness in predicting regular and explainable trends of $L_{f,50\%}$ and CV, consistent with literature data and fatigue reduction factors generally applied in machine design.

Even though the proposed model proved to be effective in the prediction of the notch fatigue strength of tool steels, it could be potentially applied to other steel grades or specimen geometry, as far as high cycle fatigue failures originate from surface defects. Future works will be focused on the definition of more accurate relationships between the parameters f and k, describing the size distribution of surface defects, and those commonly used for surface topology characterization, such as the average and maximum roughness R_a and R_{max}. Furthermore, the effectiveness of the model for different ranges of input variables should be investigated, as well as for different alloys, fatigue test conditions and notch geometry.

ACKNOWLEDGMENTS

This research did not receive any specific grant from funding agencies in the public, commercial, or not-for-profit sectors. The authors wish to thank Dr. Andrea Morri at Industrial Research Centre for Advanced Mechanics and Materials (CIRI-MAM) of the University of Bologna for his valuable support to the experimental work and Dr. Simone Messieri at Ducati Motor Holding S.p.A. for the fruitful discussion. Open Access Funding provided by Universita di Bologna within the CRUI-CARE Agreement.

DATA AVAILABILITY STATEMENT

The data required to reproduce the findings reported in the present work are available in the diagrams, tables, and images of this manuscript.

TABLE OF NOMENCLATURE

$area$	Defect area projected on the plane of maximum stress	(μm2)
$\sqrt{area}$	Defect size parameter	(μm)
$\sqrt{area}_c$	Critical size parameter for propagation	(μm)
CV	Coefficient of variation	(−)
d_{notch}	Notch-tip diameter	(mm)
E	Elastic modulus	(GPa)
f	Intercept of $N_{L(x)}$ function	(mm^{-1})
G	Normal function	(−)
HV	Vickers hardness	($kgf{\cdot}mm^{-2}$)
k	Rate of decrease of $N_{L(x)}$ function	(μm^{-1})
K_t	Theoretical stress-concentration factor	(−)
$L_{f,50\%}$	Notch fatigue strength at 10^7 cycles and 50% probability of failure	(MPa)
$N_{L(x)}$	Size distribution of surface defects	(mm^{-1})
$N_{L(\sqrt{area}_c)}$	Number of critical surface defects per unit length	(mm^{-1})
PDF	Density function of failure probability	(−)

(Continues)

P_f	Probability of failure (cumulative)	(−)
R	Stress ratio	(−)
R_a	Average roughness	(μm)
R_{max}	Maximum roughness	(μm)
SD	Standard deviation of normal function G	(MPa)
UTS	Ultimate tensile strength	(MPa)
Z	Calibration parameter	(MPa·m$^{1/2}$)
x	Arbitrary defect size	(μm)
ΔK	Stress-intensity factor range	(MPa·m$^{1/2}$)
ΔK_{th}	Fatigue threshold	(MPa·m$^{1/2}$)
$\Delta\sigma$	Stress range	(MPa)
$\Delta\sigma_{eff}$	Effective stress range	(MPa)
ν	Poisson's ratio	(−)
λ_c	Expected number of critical defects	(−)
σ_m	Mean stress over the load cycle on the notch-tip surface	(MPa)
σ_{max}	Maximum stress over the load cycle on the notch-tip surface	(MPa)
σ_{min}	Minimum stress over the load cycle on the notch-tip surface	(MPa)
σ_{nom}	Nominal stress amplitude applied in rotating bending fatigue tests	(MPa)
σ_{res}	Surface residual stress	(MPa)
μ	Mean value of normal function G	(MPa)

ORCID

Alessandro Morri https://orcid.org/0000-0002-7062-2951

REFERENCES

1. BS EN ISO 4957:2000. Tool steels. 2000.
2. Roberts G, Krauss G, Kennedy R. Tool steels: 5th edition. *Book*. 1998;121.1–6.
3. Molinari A, Pellizzari M, Gialanella S, Straffelini G, Stiasny KH. Effect of deep cryogenic treatment on the mechanical properties of tool steels. *J Mater Process Technol*. 2001;118(1-3):350-355.
4. Pellizzari M, Cescato D, de Flora MG. Hot friction and wear behaviour of high speed steel and high chromium iron for rolls. *Wear*. 2009;267(1-4):467-475.
5. Pellizzari M, Molinari A, Straffelini G. Tribological behaviour of hot rolling rolls. *Wear*. 2005;259(7-12):1281-1289.
6. Ceschini L, Morri A, Morri A, Messieri S. Replacement of nitrided 33CrMoV steel with ESR hot work tool steels for motorsport applications: microstructural and fatigue characterization. *J Mater Eng Perform*. 2018;27(8):3920-3931.
7. ISO. ISO 12107:2012 - Metallic materials - Fatigue testing - Statistical planning and analysis of data. 2012.
8. Susmel L. Fundamentals of fatigue assessment. In: Susmel L, ed. *Multiaxial Notch Fatigue*. Woodhead Publishing; 2009: 33-97.
9. Pang JC, Li SX, Wang ZG, Zhang ZF. General relation between tensile strength and fatigue strength of metallic materials. *Mater Sci Eng A*. 2013;564:331-341.
10. Murakami Y. *Metal Fatigue*. Elsevier; 2002.
11. Budynas GR, Nisbett JK. *Shigley's Mechanical Engineering Design*. Ninthed; 2011.
12. Meurling F, Melander A, Tidesten M, Westin L. Influence of carbide and inclusion contents on the fatigue properties of high speed steels and tool steels. *Int J Fatigue*. 2001;23(3): 215-224.
13. Sohar CR, Betzwar-Kotas A, Gierl C, Weiss B, Danninger H. Fractographic evaluation of gigacycle fatigue crack nucleation and propagation of a high Cr alloyed cold work tool steel. *Int J Fatigue*. 2008;30(12):2191-2199.
14. Shiozawa K, Morii Y, Nishino S, Lu L. Subsurface crack initiation and propagation mechanism in high-strength steel in a very high cycle fatigue regime. *Int J Fatigue*. 2006;28(11):1521-1532.
15. Ebara R. Some influencing variables on internal fatigue crack initiation in structural materials. *Procedia Eng*. 2016;160:21-28.
16. Chapetti MD, Tagawa T, Miyata T. Ultra-long cycle fatigue of high-strength carbon steels part I: Review and analysis of the mechanism of failure. *Mater Sci Eng a*. 2003;356(1-2):227-235.
17. Zerbst U, Klinger C. Material defects as cause for the fatigue failure of metallic components. *Int J Fatigue*. 2019;127:312-323.
18. Tanaka K, Akiniwa Y. Fatigue crack propagation behaviour derived from S-N data in very high cycle regime. *Fatigue Fract Eng Mater Struct*. 2002;25(8-9):775-784.
19. Chan KS. Roles of microstructure in fatigue crack initiation. *Int J Fatigue*. 2010;32(9):1428-1447.
20. Krewerth D, Lippmann T, Weidner A, Biermann H. Influence of non-metallic inclusions on fatigue life in the very high cycle fatigue regime. *Int J Fatigue*. 2016;84:40-52.
21. Torres Y, Rodríguez S, Mateo A, Anglada M, Llanes L. Fatigue behavior of powder metallurgy high-speed steels: Fatigue limit prediction using a crack growth threshold-based approach. *Mater Sci Eng A*. 2004;387–389:501-504.
22. Jesner G, Marsoner S, Schemmel I, Pippan R. Fatigue and fracture processes in high performance PM tool steels. *Fract Nano Eng Mater Struct - Proc 16th Eur Conf Fract*. 2006;199.
23. Lai J, Huang H, Buising W. Effects of microstructure and surface roughness on the fatigue strength of high-strength steels. *Procedia Struct Integr*. 2016;2:1213-1220.
24. Li C, Dai W, Duan F, Zhang Y, He D. Fatigue life estimation of medium-carbon steel with different surface roughness. *Appl Sci*. 2017;7(4):338.
25. Zerbst U, Madia M, Klinger C, Bettge D, Murakami Y. Defects as a root cause of fatigue failure of metallic components. *I: Basic Aspects Eng Fail Anal*. 2019;97:777-792.
26. Zerbst U, Madia M, Klinger C, Bettge D, Murakami Y. Defects as a root cause of fatigue failure of metallic components. III: cavities, dents, corrosion pits, scratches. *Eng Fail Anal*. 2019; 97:759-776.
27. Arola D, Williams C. Estimating the fatigue stress concentration factor of machined surfaces. *Int J Fatigue*. 2002;24(9): 923-930.

28. Field M, Kahles JF, Koster WP. Surface finish and surface integrity. In: *ASM Handbook*. Vol.16:19-36.
29. Deng G, Nagamoto K, Nakano Y, Nakanishi T. Evaluation of the Effect of Surface Roughness on Crack Initiation Life. *12th Int Conf Fract 2009, ICF-12*. 2009. 2
30. Landes JD, Becker WT, Shipley RS, Raphael J. Stress analysis and fracture mechanics. In: *ASM Handbook*. Vol.11; 2002: 460-483.
31. Pilkey WD. Stress concentration. In: *Formulas for Stress, Strain, and Structural Matrices*. Hoboken, NJ, USA: John Wiley & Sons, Inc.; 2009:255-305.
32. Suhr RW. The effect of surface finish on high cycle fatigue initiation in low alloy steel. In: Miller KJ, de los Rios ER, eds. *The Behaviour of Short Fatigue Cracks*. London: EGF Publication 1, Mechanical Engineering Publications; 1986: 69-86.
33. Bagherifard S, Colombo C, Guagliano M. Application of different fatigue strength criteria to shot peened notched components. Part 1: fracture mechanics based approaches. *Appl Surf Sci*. 2014;289:180-187.
34. Branco R, Costa JD, Antunes FV, Bento P. Comparative analysis of fatigue life predictions in lateral notched round bars under multiaxial loading. *Tech Mech*. 2014;34:128-141.
35. Dabiri M, Björk T. Fatigue analysis of notched specimens made of direct-quenched ultra-high-strength steel under constant amplitude loading. *Procedia Struct Integr*. 2017;5:385-392.
36. Liao D, Zhu SP, Qian G. Multiaxial fatigue analysis of notched components using combined critical plane and critical distance approach. *Int J Mech Sci*. 2019;160:38-50.
37. Liu Y, Deng C, Gong B. Discussion on equivalence of the theory of critical distances and the coupled stress and energy criterion for fatigue limit prediction of notched specimens. *Int J Fatigue*. 2020;131:105326.
38. Luo P, Yao W, Susmel L, Li P. Prediction methods of fatigue critical point for notched components under multiaxial fatigue loading. *Fatigue Fract Eng Mater Struct*. 2019;42(12):2782-2793.
39. Zhao P, Lu TY, Gong JG, Xuan FZ. A modified stress field intensity approach for fatigue life prediction of components. *Mater des*. 2020;190:108537.
40. Liao D, Zhu SP. Energy field intensity approach for notch fatigue analysis. *Int J Fatigue*. 2019;127:190-202.
41. Molski K, Glinka G. A method of elastic-plastic stress and strain calculation at a notch root. *Mater Sci Eng*. 1981;50(1): 93-100.
42. Glinka G. Energy density approach to calculation of inelastic strain-stress near notches and cracks. *Eng Fract Mech*. 1985; 22(3):485-508.
43. Lazzarin P, Zambardi R. A finite-volume-energy based approach to predict the static and fatigue behavior of components with sharp V-shaped notches. *Int J Fract*. 2001;112(3): 275-298.
44. Hu Z, Berto F, Hong Y, Susmel L. Comparison of TCD and SED methods in fatigue lifetime assessment. *Int J Fatigue*. 2019; 123:105-134.
45. Melander A, Haglund S. A NEM model for fatigue failure due to carvide cluster. *6th Int Tool Conferece - Vol II*. 2002; 699-710.
46. Nakatani M, Masuo H, Tanaka Y, Murakami Y. Effect of surface roughness on fatigue strength of Ti-6Al-4V alloy manufactured by additive manufacturing. *Procedia Struct Integr*. 2019;19:294-301.
47. BS ISO 14707: 2021. Surface chemical analysis — Glow discharge optical emission spectrometry (GD-OES) — Introduction to use. 2021.
48. BS EN ISO 6507-1L:2018 : Metallic Materials - Vickers Hardness Test. 2018.
49. BS ISO 1143:2010. Metallic materials — Rotating bar bending fatigue testing. 2010.
50. Noda N, Takase Y. Stress concentration formula useful for all notch shape in a round bar (comparison between torsion, tension and bending). *Int J Fatigue*. 2006;28(2):151-163.
51. DIN 4768:1990 Determination of surface roughness values of the parameters Ra, Rz, Rmax by means of electrical contact (stylus) instruments; terminology, measuring conditions. 1990.
52. European Committee for Standardization EN 13925 Non-Destructive Testing - X-Ray Diffraction from Polycrystalline and Amorphous Materials. 2003.
53. Yin GQ, Kang X, Zhao GP. Fatigue properties of the ultra-high strength steel TM210A. *Materials*. 2017;10(9):1057.
54. BS EN ISO 4287:1998. Geometrical Product Specification (GPS) - Surface Texture: Profile Method - Terms, Definitions and Surface Texture Parameters. 2009.
55. Perez N. *Fracture Mechanics*. Cham: Springer International Publishing; 2017.
56. Roiko A, Murakami Y. A design approach for components in ultralong fatigue life with step loading. *Int J Fatigue*. 2012;41: 140-149.
57. Borsato T, Ferro P, Fabrizi A, Berto F, Carollo C. Long solidification time effect on solution strengthened ferritic ductile iron fatigue properties. *Int J Fatigue*. 2021;145:106137.
58. Tang K, Du Z, Ferro P, Berto F. Crack initiation and propagation from geometric microdefects: Experiment and transition fatigue behavior. *Fatigue Fract Eng Mater Struct*. 2021.44(9): 2323–2336.
59. Romano S, Brückner-Foit A, Brandão A, Gumpinger J, Ghidini T, Beretta S. Fatigue properties of AlSi10Mg obtained by additive manufacturing: defect-based modelling and prediction of fatigue strength. *Eng Fract Mech*. 2018;187:165-189.
60. Romano S, Nezhadfar PD, Shamsaei N, Seifi M, Beretta S. High cycle fatigue behavior and life prediction for additively manufactured 17-4 PH stainless steel: effect of sub-surface porosity and surface roughness. *Theor Appl Fract Mech*. 2020;106: 102477.
61. Lawson L, Chen E, Meshii M. Near-threshold fatigue: a review. *Int J Fatigue*. 1999;21:15-34.
62. Taylor D. *Fatigue Thresholds*. Butterworths; 1989.
63. Taylor D. Fatigue thresholds: their applicability to engineering situations. *Int J Fatigue*. 1988;10(2):67-79.
64. Ritchie RO. Near-threshold fatigue-crack propagation in steels. *Int Met Rev*. 1979;24(1):205-230.
65. Paolino DS, Tridello A, Chiandussi G, Rossetto M. Effect of defect size on P-S-N curves in very-high-cycle fatigue. *Procedia Struct Integr*. 2017;7:335-342.
66. Gao X, Caivano R, Tridello A, et al. Innovative formulation for topological fatigue optimisation based on material defects distribution and TopFat algorithm. *Int J Fatigue*. 2021;147:106176.
67. Paolino DS, Tridello A, Chiandussi G, Rossetto M. Estimation of P-S-N curves in very-high-cycle fatigue: statistical procedure

based on a general crack growth rate model. *Fatigue Fract Eng Mater Struct*. 2018;41(4):718-726.
68. Paolino DS. Very high cycle fatigue life and critical defect size: modeling of statistical size effects. *Fatigue Fract Eng Mater Struct*. 2021;44(5):1209-1224.
69. Chapetti MD. Prediction of threshold for very high cycle fatigue (N>107 cycles). *Procedia Eng*. 2010;2(1):257-264.
70. McEvily AJ, Endo M, Murakami Y. On the relationship and the short fatigue crack threshold. *Fract Eng Mater Struct*. 2003; 26:269-278.
71. Maierhofer J, Gänser H-P, Pippan R. Modified Kitagawa–Takahashi diagram accounting for finite notch depths. *Int J Fatigue*. 2015;70:503-509.
72. Minakawa K, McEvily AJ. On crack closure in the near-threshold region. *Scr Metall*. 1981;15(6):633-636.
73. Bagherifard S, Guagliano M. Application of different fatigue strength criteria on shot peened notched parts. Part 2: Nominal and local stress approaches. *Appl Surf Sci*. 2014;289: 173-179.
74. Kostilnik T. Shot peening. In: *ASM Handbook*. Vol.5:126-135.
75. Sawada T, Yanagitani A. Properties of cold work tool steel shot peened by 1200 HV-class Fe-Cr-B gas atomized powder as shot peening media. *Mater Trans*. 2010;51(4):735-739.

How to cite this article: Zanni M, Morri A, Ceschini L. Development and validation of a probabilistic model for notch fatigue strength prediction of tool steels based on surface defects. *Fatigue Fract Eng Mater Struct*. 2022;45(1):113-132. doi:10.1111/ffe.13588